CrystEngComm

RSC Publishing

HIGHLIGHT

View Article Online
View Journal | View Issue

Cite this: *CrystEngComm*, 2013, **15**, 3058

Halogen bonding at work: recent applications in synthetic chemistry and materials science

Franck Meyer*[a] and Philippe Dubois[b]

Received 15th July 2012,
Accepted 13th August 2012

DOI: 10.1039/c2ce26150b

www.rsc.org/crystengcomm

Halogen bonding has recently entered the arena of reliable and valuable non-covalent interactions for the construction of supramolecular complexes. A step further, this highlight provides some new insights related to the design of advanced functional materials encompassing halogen bonded mesomorphic and electronic components. Other recent applications have been extended to various aspects of solution phase recognition (catalysis, ion sensing and resolution) and macromolecular organizations (porous, polymeric and hybrid systems).

Introduction

Supramolecular chemistry relies on molecular recognition processes allowing the self-organization of components by non-covalent forces. Initially, this elegant mechanism aimed at mimicking biological systems through the rational design of complementary molecular entities. However, the rise of the supramolecular approach was implemented by the concept of molecular information. Thus, the transfer of structural features from a molecular component to the supramolecular level permitted the elaboration of complex architectures and devices. Beyond the self-organization of selected partners, the design of purpose-built and programmed compounds thereby provides solutions to specific research areas giving access to advanced functional materials and other useful applications.[1]

The principle of complementarity in the creation of host-guest systems has brought out a large array of non-covalent bonds, namely hydrogen bonding, π–π and van der Waals interactions and electrostatic forces. Recently, the supramolecular toolbox has been reinforced by a new item: halogen bonding (XB).[2] As a counterpart of hydrogen bonding (HB), halogen bonding encompasses any type of non-covalent interactions involving a halogen atom as an acceptor of electronic density. Although seemingly new at first glance, the use of halogen atoms as recognition sites was already reported in the 1960's.[3] At the tail end of the 1990's, G. Resnati rediscovered this weak interaction, operating a dramatic and fruitful shift toward the solid state supramolecular chemistry. At this stage, XB has emerged as a reliable driving force in the construction of self-assembled architectures and arisen as a strong, specific, and highly directional interaction. During the last decade, halogen bonded systems have attracted a steady interest with the group of Resnati and Metrangolo at the forefront. Slowly, XB based recognition processes have moved from crystal engineering to functional materials. In this highlight, we decided to shed some light on recent applications of XB where specific properties stem from the rational design of components. This overview will tackle a vast area of research themes, namely the soft and electronic materials, anion sensing, scavenging systems, polymer and nanoparticle organizations, the solid-state synthesis, catalytic, recycling and resolution processes.

Despite being of relevant interest in biological systems, the occurrence of XB in protein–ligand interactions and related drug design is actually well-documented in other reviews and therefore, these topics will be absent from this manuscript.[4] Likewise, the main features regarding crystal engineering based scaffolds and the nature of XB have also been discussed in details elsewhere.[5]

Liquid crystals

In the landscape of non-covalent interactions, the halogen bonding appeared to be a very appealing strategy in the design of new soft materials. Taking note of the analogy between hydrogen bonding and halogen bonding and the predominant role of haloperfluorocarbons in XB systems, the elaboration of supramolecular liquid crystals (LCs) was performed by the self-assembly through N···I interactions of alkoxystilbazoles (**St**) and the iodopentafluorobenzene (**IPFB**) (Fig. 1). After the slow evaporation of a solution containing equimolar quantities of the two components, the single crystal X-ray diffraction analysis of one complex revealed a N···I distance of 2.811 Å and a N–I–C angle of 168.4° consistent with an electron donation from nitrogen to iodine. Then, examination of

[a]*Laboratory of Biopolymers and Supramolecular Nanomaterials, Faculty of Pharmacy, Université Libre de Bruxelles (ULB), Campus de la Plaine, Boulevard du Triomphe, 1050 Bruxelles, Belgium. E-mail: franck.meyer@ulb.ac.be*
[b]*Laboratory of Polymeric and Composite Materials, Center of Innovation and Research in Materials and Polymers (CIRMAP), University of Mons UMONS, Place du Parc 20, 7000, Mons, Belgium*

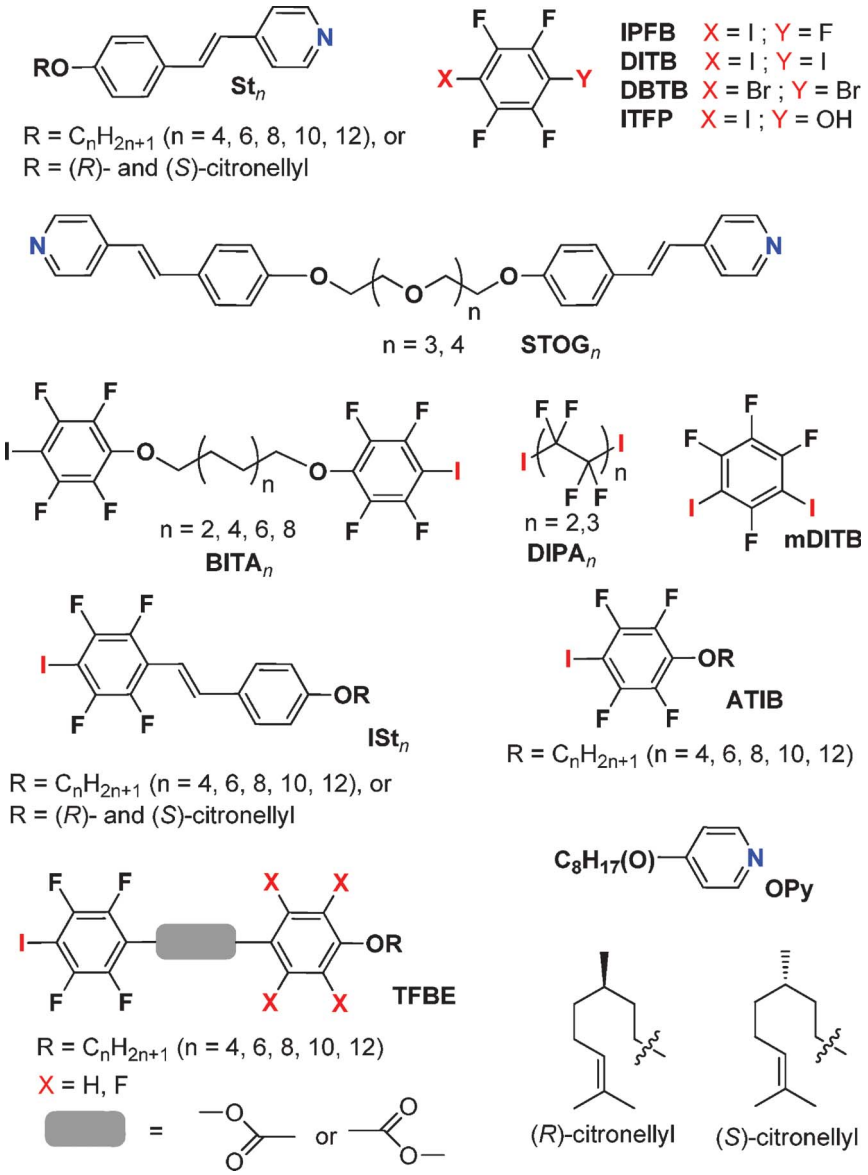

Fig. 1 Mesogens involved in XB liquid crystals.

samples by hot stage polarizing microscopy has readily evidenced thermotropic mesophases despite the non-mesomorphic nature of the starting materials. Thus, the LC phases shifted from monotropic to enantiotropic and their characters progressed from nematic to smectic.[6]

Afterward, the self-assembly of difunctional compounds has given rise to halogen-bonded polymeric liquid crystals.[7] The telechelic α,ω-bis(4-iodo-2,3,5,6-tetrafluorophenoxy) alkane derivatives (**BITA**) were associated with stilbazole units appended to oligoglycol spacers (**StOG**) (Fig. 1). Complexes have endowed monotropic liquid crystallinity on cooling, featuring typical droplet nematic phases. Subsequent works have reported the construction of trimeric systems involving alkoxystilbazoles as electron donors. First, 2 : 1 mixtures were prepared by the association of previous iodo derivatives **BITA** with two stilbazoles **St** (Fig. 1). Samples were characterized by X-ray photoelectron spectroscopy (XPS) and IR analyses, confirming the effective complex formation.[8] With the exception of three compounds, their thermal behaviour has revealed a predominant monotropic SmA mesomorphism whose main feature lied in constant melting and clearing unrelated to the size of the building blocks. A second approach has concerned the association of telechelic α,ω-diiodoperfluoroalkanes (**DIPA**) and stilbazoles **St** (Fig. 1).[9] The X-ray diffraction of **St$_8$-DIPA$_3$** highlighted an effective segregation of perfluoroalkyl and stilbazole units bound by N···I interactions. With the exception of one sample, all complexes have displayed a monotropic nematic phase with LC transition in the range 4 to 8 °C. In the same spirit, investigations were pursued with trimeric systems containing stilbazoles **St** and 1,4-dihaloperfluoroarenes as ditopic linkers (**DITB** and **DBTB**) (Fig. 1).[10] In both cases, the X-ray diffraction analysis proved almost isostructural trimeric

complexes, namely a **St:DITB** (or **DBTB**) 2 : 1 ratio, but their thermal behaviour has differed dramatically. On cooling from a homogeneous isotropic state, a monotropic nematic phase was seen for the iodo derivatives **St$_n$-DITB** (n = 6, 8, 10) with thermodynamic nematic–isotropic transition around 110 °C. Regarding the non-mesomorphic bromo derivative **St$_8$-DBTB**, the absence of LC behaviour was attributed to the weaker N···Br interaction which was unable to recombine the units in the liquid phase. Further investigations allowed the formation of enantiotropic mesomorphism from **St$_n$-DITB** mixtures with a definitely wider mesophase transition for one sample (~11.5 °C).

At the same time, Bruce and co-workers proceeded with bent-core liquid crystals.[11] The most attractive aspects of these mesomorphic materials lie in chirality and polarity, despite being formed from achiral entities. The co-crystallization of alkoxystilbazoles **St** and 1,3-diiodotetrafluorobenzene (**mDITB**) in a 2 : 1 ratio provided suitable materials for X-ray analysis (Fig. 1). As expected, the two stilbazoles and the aromatic ring formed a V shaped structure, characterized by N···I distances approximately 20% shorter than the sum of the van der Waals radii, associated with almost linear C–N–I angles. As far as the liquid crystalline behaviour is concerned, differential scanning calorimetry (DSC) and polarizing optical microscopy studies confirmed a monotropic mesomorphism on cooling. An isotropic to nematic phase transition was observed in addition to a nematic to chiral nematic sequence. This spontaneous symmetry-breaking in halogen bonded bent-core materials provided the first chiral XB mesophases formed from achiral starting units.

Keeping in mind a potential complementarity between hydrogen and halogen bonding, experiments aiming at combining both interactions were carried out.[12] Typically, 4-iodotetrafluorophenol (**ITFP**) was challenged with a set of 4-alkoxystilbazoles **St** in a 1 : 2 ratio in THF (Fig. 1).[13] The single crystal X-ray analysis showed that the three components are almost co-planar, connected by N···I and N···H bonds. The transition temperatures, as obtained by polarizing optical microscopy, revealed a monotropic nematic phase for the short-chain homologue **St$_4$-ITFP** while higher analogues **St$_n$-ITFP** (n = 6, 8, 10) turned to an enantiotropic mesomorphism; a smectic A phase was seen for **St$_{12}$-ITFP**. Interestingly, the nematic phase transition dropped sharply as the chain length of **St** increased (n = 6 to 10).

Finally, an impressive set of 90 dimeric systems was studied in order to provide new insights on structure/mesomorphism relationships.[14] Mesogens consisted in a combination of 4-substituted pyridines and 4-substituted iodotetrafluorobenzene (Fig. 1). First, 1 : 1 complexes comprising alkoxystilbazoles **St** and *trans*-stilbene derivatives (**ISt**) as XB donors were obtained by co-crystallization of an equimolar amount of each component. In both cases, the aromatic rings are appended to achiral alkyl chains or chiral citronellyl groups (R and S enantiomers).

The mesomorphic properties of achiral series **St$_n$-ISt$_n$** lied mainly in an enantiotropic behaviour dominated by nematic phases for short to medium chain length. For the longest chain lengths, a monotropic SmA phase was developed and progressed enantiotropically (Fig. 2). As concerns the chiral analogues (**St$_n$-ISt$_{R/S}$**, **St$_{R/S}$-ISt$_n$**, and **St$_{R/S}$-ISt$_{R/S}$**), enantiotropic chiral nematic mesophases were seen in most samples and only a few chiral smectic A phases. It is noteworthy that enantiomeric couples demonstrated similar mesomorphic behaviours. In addition, a variation of chain length in systems **St-ISt** accounted for a thin modulation of mesomorphic properties. The second part dealt with complexes formed of alkoxystilbazoles **St$_n$** and alkoxytetrafluoroiodobenzenes (**ATIB**). The thermal data for these complexes presented exclusively a SmA phase and only two complexes revealed an enantiotropic mesophase. New two ring-containing ester compounds **TFBE** were also evaluated as XB donors toward stilbazoles **St** and octylpyridines **OPy**. The majority of these complexes exhibited a monotropic phase which was, in most cases, nematic.

Non-linear optical, photoresponsive and phosphorescent materials

A great deal of effort has been devoted to the elaboration of new materials exhibiting second-order nonlinear optical (NLO) properties. Typically, the structure of chromophores is based upon π-conjugated organic systems unsymmetrically end-capped with electron donor and acceptor functions to impart the electronic bias. In order to extend the self-assembled properties of XB to electrooptical materials, the molecular design of chromophores incorporating halogen bond donor groups was studied.[15] Self-complementary components *N*,*N*-dimethyl-4-[(E)-2-(2,3,5,6-tetrafluoro-4-iodophenyl)vinyl]aniline (**DMIA**) and *N*,*N*-dimethyl-4-[(1E,3E)-4-(2,3,5,6-tetrafluoro-4-iodophenyl)buta-1,3-dien-1-yl]aniline (**DMBAa**) were synthesized and compared to *N*,*N*-dimethyl-4-[(1E,3E)-4-(2,3,5,6-tetrafluorophenyl)buta-1,3-dien-1-yl]aniline (**DMBAb**) (not capable of XB) (Fig. 3). The evaluation of their NLO responses at molecular level by electric field induced second harmonic generation (EFISH) experiments appeared solvent dependent. In chloroform, $\mu\beta$ values were in the range +124 to +192 × 10^{-48} esu which was in sharp contrast with results obtained in DMF. Indeed, EFISH values for XB NLO-phores **DMIA** and **DMBAa** came out negative (−465 × 10^{-48} esu for

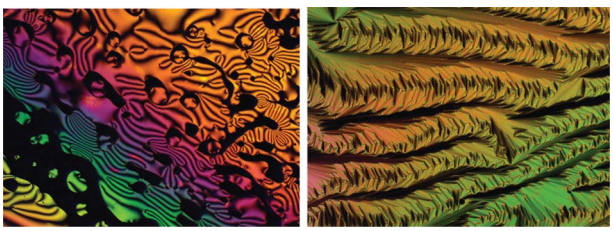

Fig. 2 Nematic phase (left) and smectic A phase (right) observed for St_4-ISt_4 (reproduced with permission from John Wiley and Sons).

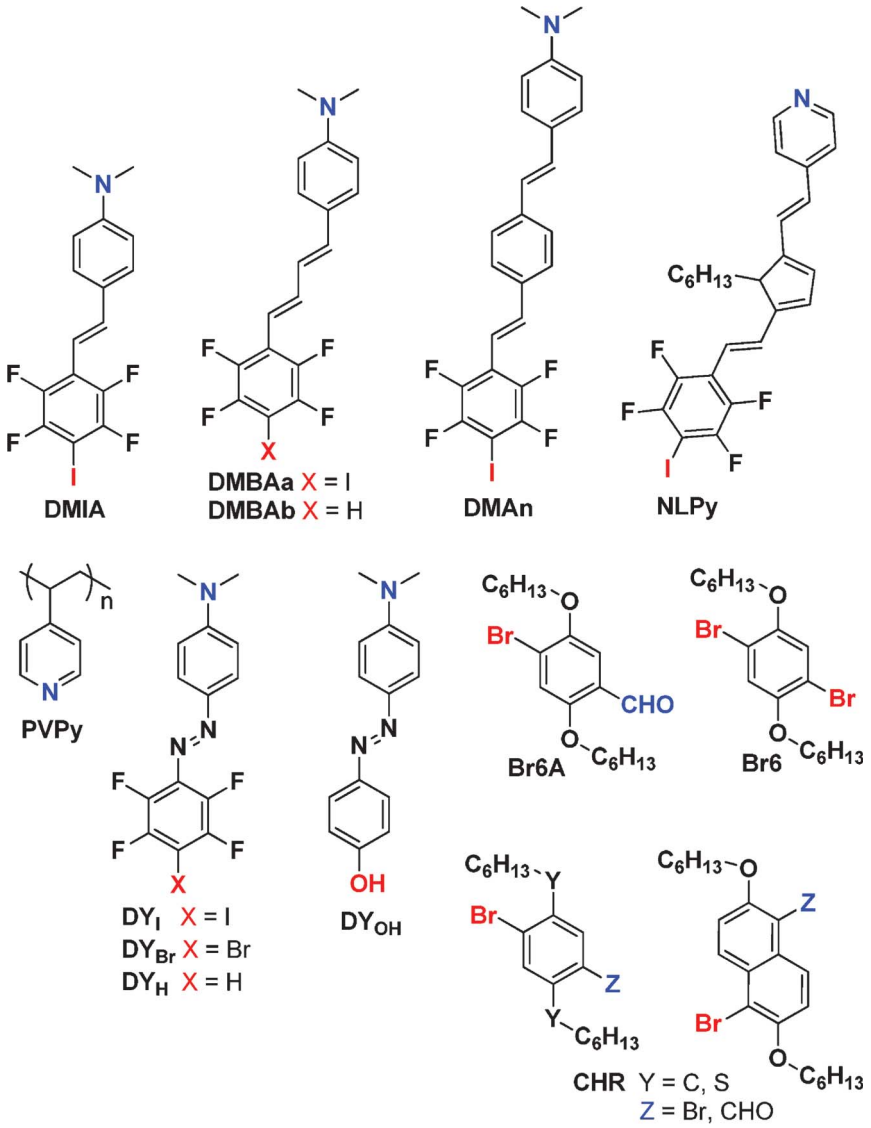

Fig. 3 Structures of non-linear optical, photoresponsive and phosphorescent materials.

DMBAa) whereas the $\mu\beta$ value for compound **DMBAb** remained positive (+70 × 10^{-48} esu). Thus, the tuning effect of the NLO response was attributed to an inversion of the dipole moment μ owing to halogen bonded solvent··· chromophore interactions (C=O···I), which was also supported by DFT calculation. In light of these observations, new self-complementary tectons **DMAn** and **NLPy** were prepared and the EFISH study has provided the same inversion of $\mu\beta$ values from positive to negative on going to chloroform to DMF (+700 to −2000 × 10^{-48} esu for **DMAn**) (Fig. 3).[16]

Recently, XB was investigated in the field of light induced surface patterning featuring azobenzene-containing polymers. Purposely, poly(4-vinylpyridine) (**PVPy**) and different dyes **DY** allowing either XB or HB interactions were combined for the design of photoresponsive polymers $(\mathbf{PVPy{\cdot}DY})_x$ (x = dye/polymer ratios) (Fig. 3). According to XPS analyses of spin cast films, a shift of binding energies for a I3d doublet in $(\mathbf{PVPy{\cdot}DY_I})_{0.2}$ and O1s electron in $(\mathbf{PVPy{\cdot}DY_{OH}})_{0.2}$ attested to the supramolecular character of the photoresponsive materials. Subsequently, the first-order diffraction efficiency evolution of $(\mathbf{PVPy{\cdot}DY})_{0.1}$ appeared as follows: $\mathbf{DY_I} > \mathbf{DY_{OH}} > \mathbf{DY_{Br}} > \mathbf{DY_H}$. Moreover, the modulation depths of the gratings for complexes $(\mathbf{PVPy{\cdot}DY_I})_{0.2}$ and $(\mathbf{PVPy{\cdot}DY_{OH}})_{0.2}$ were ∼90 nm and 70 nm in favour of the XB device. Hence, the overall surface relief gratings efficiency seemed to be highly dependent of the directionality of the non-covalent interaction, one of the main features of halogen bonding.[17]

In 2011, the phosphorescence of purely organic crystals was found to be dependent of halogen bonding. Under 360 nm excitation of crystals of 2,5-dihexyloxy-4-bromobenzaldehyde (**Br6A**), a strong green phosphorescence is emitted at 500 nm presumably owing to the very short C=O···Br contacts observed in the crystal packing (Fig. 3). In order to get rid of the self-quenching, the dilution of compound **Br6A** with 2,5-dihex-

yloxy-1,4-dibromobenzene (**Br6**) (non-emissive compound but capable of XB) in ~0.001 to ~1 wt% has given rise to green phosphorescent solids. Diluted phosphor **Br6A** has resulted as a much more efficient emitter with a shift of phosphorescent quantum yields and lifetimes from 2.9 to 55 ± 3% and 5.4 to 8.3 ms, respectively, with respect to the pure form. A step further, the association of guest aldehyde **Br6A** (~1wt%) with different designed chromophores **CHR** as XB host partners allowed a thin modulation of electron density and provided new phosphorescent materials with green, orange, yellow and blue photoluminescence emissions (Fig. 4).[18]

Magnetic and conducting materials

In the early 1990's, several research groups exploited the intermolecular self-assembly properties of XB for the construction of magnetic and conducting materials.[19] In general, the starting units encompass neutral nitroxide free radicals or ferromagnetic ions for magnetic materials and organic conductors based on tetrathiafulvalenes (TTFs) for conducting systems. Some documents have thoroughly reviewed these works and therefore we decided to pick up only a recent example exhibiting both properties.[20] Keeping in mind the scope of this highlight, the following work reported not only the crystal structures of halogen bonded complexes but also the physical properties that stem from these specific organizations. Thus, Fourmigué and co-workers have explored the electrocrystallization of donor molecule 3,4-diiodo-3′,4′-ethylenedithiotetrathiafulvalene (**EDT-TTFI$_2$**) with inorganic perchlorate ions (**ClO$_4^-$**) and various organic sulfonates, *i.e.* racemic camphor sulfonate (**RCS**), 1,5- and 2,6-naphtalene bis(sulfonate) (**1,5NS** and **2,6NS**), and 2,6-anthracene bis(sulfonate) (**2,6AS**) (Fig. 5). X-ray structures of **EDT-TTFI$_2$·ClO$_4^-$** and **EDT-TTFI$_2$·2,6NS** were consistent with ρ = 1 charge transfer whereas complexes with **RCS**, **1,5NS** and **2,6AS** endowed an averaged usual oxidation state ρ = 0.5. Iodinated **EDT-TTFI$_2$** were bound by sulfonate ions owing to short I···O intermolecular interactions and additional S···S interactions also participated to the rise of magnetic and conducting properties. As concerns the electronic behaviour of **EDT-TTFI$_2$** salts, the temperature dependence of the magnetic susceptibility of **EDT-TTFI$_2$·ClO$_4^-$** and **EDT-TTFI$_2$·2,6NS** complexes fulfilled a Curie-type law including 0.3 and 1.3% paramagnetic defaults, respectively, in line with the dimerization of the cation radicals. Unlike, complexes comprising **RCS**, **2,6AS** and **1,5NS** sulfonates have endowed room temperature conductivities ranging 6–30 × 10^{-3} to 8 S cm^{-1}. The temperature dependence of the magnetic susceptibility of these salts revealed a thermally activated semiconducting behaviour.[21]

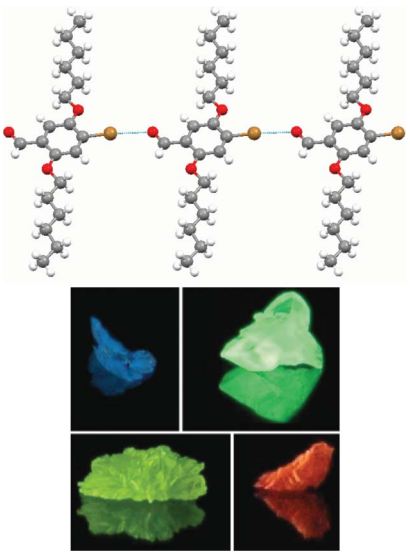

Fig. 4 X-Ray structure of **Br6A** (top). Colours are as follow: C, grey; H, white; O, red; Br, brown. Halogen bonds are dotted blue lines. Color change by modification of core structure of **CHR** (bottom). Reproduced with permission from Nature Publishing Group.

Anion sensing

The selective recognition of anions appears of fundamental importance in many biological, chemical, and environmental processes. Thus, the development of solution-phase anion receptors based on XB makes sense since anions have already demonstrated a high ability in governing supramolecular architectures.[22] In 2005, the design of a tripodal receptor **POD** possessing tetrafluoroiodobenzene groups on chain end was thought-up (Fig. 6). In the presence of NaI, the I$^-$···I interactions have conducted to the formation of a supramolecular complex where the sodium cation sits in the middle of the tritopic host, as shown by X-ray diffraction analysis. In solution, competitive tandem ESI-MS/MS experiments have clearly highlighted a higher affinity of **POD** for iodide anion over bromide and chloride anions (Fig. 7).[23]

In the same vein, a new system based on *ortho*-substituted iodoperfluoroarenes was developed (Fig. 6). The receptor-binding ability of **oTFIB** was first identified in solution by ^{19}F NMR experiments in the presence of tetrabutyl ammonium salts: characteristic downfield shifts have resulted upon XB interactions. Subsequently, binding constants were determined in solution, giving rise to a predominant association between **oTFIB** and chloride anion (K_a = 1.9·10^4 M^{-1}). The preference of the XB donor for the anions appeared as follows: Cl$^-$ > Br$^-$ > I$^-$ >>> TsO$^-$, NO$_3^-$, HSO$_4^-$.[24] Then, Taylor and co-workers have developed new systems based on urea receptors where hydrogen bonding and halogen bonding act in concert (Fig. 6). Ethanolamine based compounds incorporating iodoperfluoroaryl groups and its perfluorinated analog were studied in anion and oxoanion recognition by ^{1}H and ^{19}F NMR. Thus, the presence of an XB donor group on receptor **URa** conferred a significant level of halide selectivity (Cl$^-$ > Br$^-$ > I$^-$) in comparison to **URb**. Furthermore, the binding data for dihydrogenphosphate (H$_2$PO$_4^-$) corroborated the occurrence of XB in controlling the conformation of adjacent DNA oligomers.[25] Following a new design principle, a small

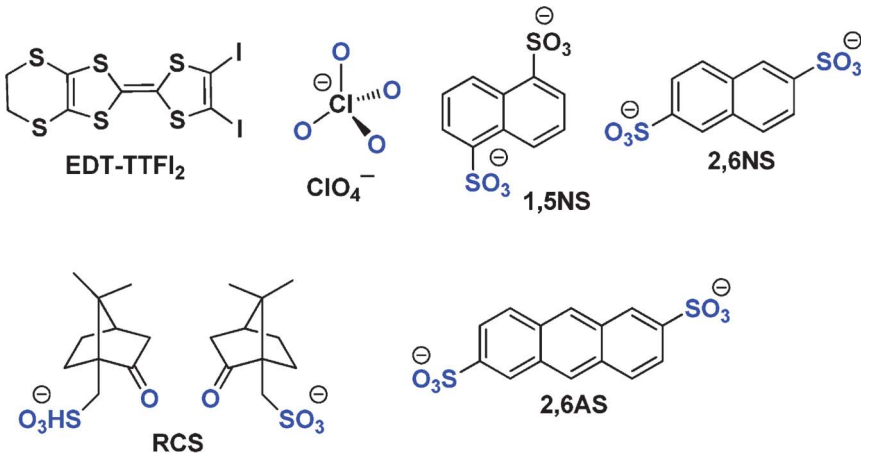

Fig. 5 Structures of components exhibiting magnetic and conducting properties.

series of bromo- and hydroimidazoliophane receptors **IMa-c** were synthesized with bromide and hexafluorophosphate counteranions (Fig. 6). The single crystal analysis of both *syn* and *anti* PF_6^- salts **IMa** revealed weak to negligible $Br\cdots PF_6^-$ halogen bondings, in contrast with significant $Br\cdots Br^-$ interactions in *syn* and *anti* bromide salts **IMb** ($Br\cdots PF_6^-$ and $Br\cdots Br^-$ distances were 7% and 13% shorter than the sum of van der Waals radii, respectively). The anion-binding properties of bromo- and hydroimidazoliophane $2PF_6^-$ receptors **IMa,c** were then determined by ^1H NMR titration experiments in the presence of tetrabutylammonium fluoride, chloride, bromide, and iodide in a mixture CD_3OD/D_2O 9 : 1. Titration data correlated to a 1 : 1 host–guest binding model showed a high binding affinity of *syn* bromohydroimidazoliophane receptor **IMa** for bromide anion (K_a = 899 M^{-1}), with the following trend: $Br^- > I^- >> Cl^-$. By comparison, the hydrogen bonding counterpart **IMc** demonstrated a much smaller strength of interaction toward Br^-, I^-, and Cl^- anions with almost no selectivity.[26] It is worth noting that other investigations were also devoted to the rational design and the understanding of halogen bonding-based receptors.[27]

Porous and organic inclusion systems

Molecular imprinting and inclusion/porous complexes represent straightforward access to new devices with adaptable catalytic or molecular storage/separation properties. In 2005,

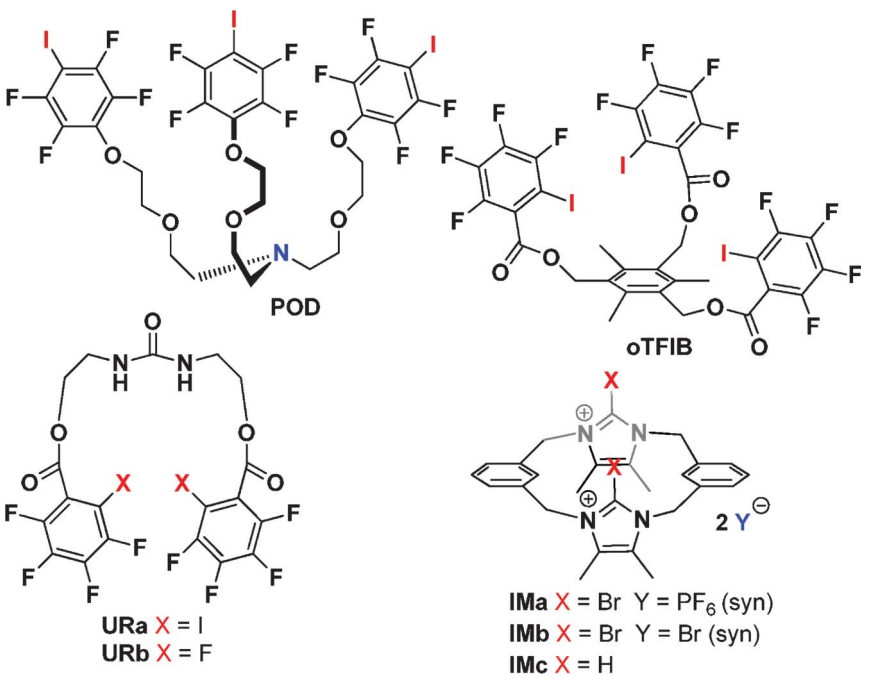

Fig. 6 Structures of receptors.

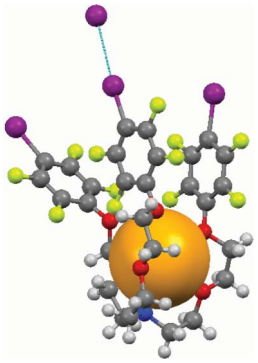

Fig. 7 X-Ray structure of tripodal receptor POD in the presence of NaI. Colours are as follow: C, grey; H, white; F, yellow; I, purple; N, blue; O, red; Na, orange. Halogen bonds are dotted blue lines.

the construction of an imprinted polymer with a selective recognition toward 4-dimethylaminopyridine (**DMAP**) was envisioned (Fig. 8). The co-polymerization of 2,3,5,6-tetrafluoro-4-iodostyrene (**TFIS**) as XB binding site, with styrene and divinylbenzene as crosslinking agents was carried out in the presence of nitrogenated template. The N···I interactions between **DMAP** and the XB donor units were expected to maintain a specific shape into the polymer matrix after removal of the dibinding-site template. In this regards, the imprinted polymer ability was measured through a competitive experiment with potential guests possessing similar functions. **DMAP** has demonstrated a higher affinity with the porous system in comparison to the other analytes with the exception of 4-aminopyridine. This selectivity (1.7 times higher than that of **DMAP**) was attributed to less steric hindrance at 4-position for 4-aminopyridine.[28]

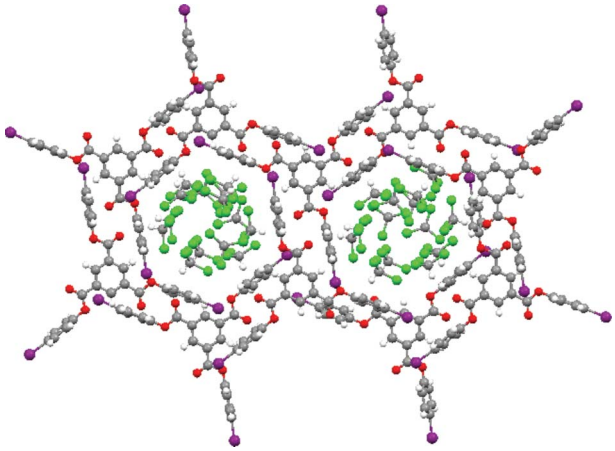

Fig. 9 X-ray structure of **TIB** with clathrated $CHCl_3$ molecules. Colours are as follow: C, grey; H, white; I, purple; O, red; Cl, green.

Later, Pigge and co-workers disclosed the inclusion capability of trigonal 1,3,5-tris(4-iodophenoxycarbonyl) benzene (**TIB**) (Fig. 8). This compound is capable of self-organization by C=O···I interactions in addition to less common π···I contacts. Thus, crystallization of (**TIB**) from chloroform has given rise to 2D layers arranged in a parallel fashion with clathrated $CHCl_3$ molecules into a hexagonal structure of diameter ~13 Å (Fig. 9).[29] Interestingly, experiments with pyridine and benzene have provided similar hexagonal patterns with a theoretical porosity of 39.7% for included pyridine sample. It is noteworthy that pyridyl groups do not disrupt the weak C=O···I and π···I interactions although numerous works accounted for N···I halogen bonds.[30]

Recently, the breathing behaviour of a hexamethylenetetramine (HMTA) and *N*-iodosuccinimide (NIS) system was

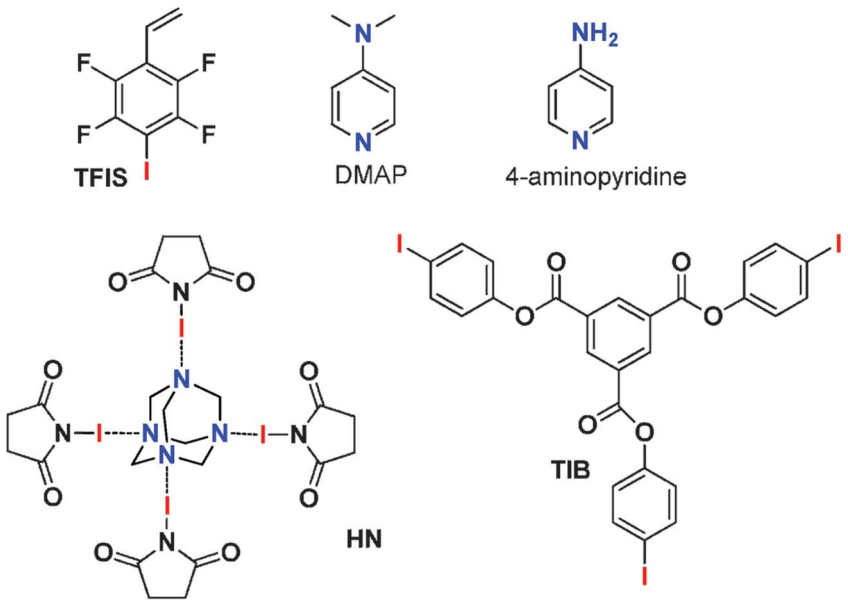

Fig. 8 Structures of units involved in porous materials.

considered as a function of solvent guests (chloroform, toluene, nitromethane, dichloromethane or tetrachloromethane).[31] Crystallographic data of all $[HMTA]\cdot[NIS]_4$ complexes (**HN**) have shown the shortest N···I distances reported to date, ranging from 26.7 to 29.6% of the sum of the van der Waals radii. Moreover, template guests enabled a thin modulation of the channel structures varying from 19.3 to 38.5% (708–1790 $Å^3$) of the unit cell volume, in the following trend: $C_6H_5CH_3 < CHCl_3 < CCl_4 < MeNO_2 < CH_2Cl_2$ (Fig. 8). Taking advantage of the same square-grid type packing in **HN**.CH_2Cl_2 and **HN**.CCl_4, a single-crystal to single-crystal transformation was operated in solution and gas phases with a preformed **HN**.CH_2Cl_2 complex. In both cases, the crystal structure of resulting complexes confirmed a guest exchange from CH_2Cl_2 to CCl_4.[32]

Film/polymer organization and nanoparticle self-assembly

The controlled surface modification is regarded as a very appealing strategy to tailor the chemical and physical properties of a substrate. In that way, the fluorinated coating of surface has been investigated through the self-assembly of poly(4-vinylpyridine) (**PVPy**) and α,ω-diiodoperfluoroalkanes **DIPA$_n$** (Fig. 10). Supramolecular complexes of **PVPy** ($M_n \sim 1800$ to 5060 g mol^{-1}) and **DIPA$_n$** were prepared in chloroform solutions with different N/I ratio (0.5–2 : 1). After evaporation of the solvent, IR and Raman analyses of paste-like residues highlighted N···I interactions by a shift for selected vibration bands of XB **PVPy·DIPA** complexes in comparison to the neat materials, also supported by thermal analysis. Beyond the formation of supramolecular fluorinated coatings, a polarizing optical microscopy study of comb-like polymer **PVPy·DIPA$_6$** ($M_n \sim 1800$) has displayed typical smectic-type liquid crystal behaviour, arising as the very first halogen bonded mesomorphic system.[33]

Layer-by-layer (LbL) assembly has gained a tremendous interest due to its capacity to achieve multilayer films with specific architectures. Purposely, a film construction by LbL assembly was studied using poly(4-(4-iodo-2,3,5,6-tetrafluorophenoxy)-butyl acrylate) (**PIPBA**) and **PVPy** on a NH_2-modified substrate (Fig. 10). Successive immersions in **PIPBA** and **PVPy** solutions (1.9×10^{-3} mol (repeat units) L^{-1}) allowed a multilayer film formation through N···I interactions, as confirmed by UV-vis absorption band at 256 nm for **PVPy** and 233 nm for **PIPBA**. The frequency shift of the quartz crystal microbalance resonator displayed a polymer bilayer content of about 255 ± 50 ng cm^{-2}. An additional XPS analysis also proved the effective XB film formation by a shift of binding energy of N 1s (BE_{N1s}) and I 3d (BE_{I3d}) with respect to pure **PIPBA** and **PVPy**, in agreement with N···I halogen bonds. Further investigations have shed light on the surface morphology and the thickness of the multilayer films. So, a root-mean-square roughness of about 0.78 nm (determined by AFM) attested for LbL assembly in flat film. Regarding the thickness of one bilayer, a value of about 1.3 ± 0.3 nm was obtained by X-ray reflection experiments.[34]

In 2008, Facchetti and van der Boom reported the thin films grown by physical vapor deposition (PVD) on bare and $Cl_3Si(CH_2)_{11}CN$-functionnalized silicon substrates of self-complementary XB tectons **NPy** and **NOI** (Fig. 10). Whatever the substrate, the AFM morphology analysis of **NPy**-based films presented a uniform grain. In contrast, the *N*-oxide derivative **NOI** exerted a high level of control over the morphology of the thin films. This was highlighted by densely packed grains observed on bare silicon substrates and uniformly distributed islands on functionalized substrates. As concerns the stilbazole derivative **NPy**, the simulated powder pattern proved identical microstructural organizations for crystals grown in solution and on the film. In contrast, arrangements with compound **NOI** appeared different and remained independent of the silicon substrate. The XB-based film growth by PVD thereby opens a very appealing strategy for the development of new organic optoelectronic materials.[35]

The bottom-up approach represents a compelling option for the creation of highly 3D organized nanostructures. In this regard, the role of halogen bonding as a structure-directing agent was studied in organic π-conjugated polymers. Organizations of poly(3-alkylthiophenes) (**P3ATs**) and brominated analogs (**P3ATBrs**) were investigated by scanning tunneling microscopy (STM) on highly oriented pyrolytic graphite (HOPG) (Fig. 10). In both systems, a well-organized structure was observed for the first layers. However, this arrangement differed dramatically at the second layer level. Indeed, samples comprising **P3ATBs** chains exhibited a good alignment and periodicity with respect to the underlying layer, in opposition to **P3ATs** samples constituted of poorly organized structures with isolated strands (Fig. 11). This 3D molecular self-assembly was attributed to S···Br halogen bonds capable of inducing a self templating effect, leading to the relative positioning of the successive layers.[36]

The formation of hybrid systems through the association of organic–inorganic components has opened a new pathway to highly functional materials. Assuming XB as a potential driving force for the self-assembly of hybrid compounds, gold-nanoparticles (**AuNPs**) were capped with XB donor moieties by displacement of tetraoctylammonium bromide for XB donor ligand **NOI** using the *N*-oxide groups as coordination sites (Fig. 10). When exposed to 1,4-bis((*E*)-2-(pyridin-4-yl)vinyl)benzene (**BPEB**), a fast aggregation of nanoparticles **AuNPs-NOI**/**BPEB** was determined by surface plasmon resonance, *i.e.* a decrease of 522 nm band and broadening of the lower-energy band at $\lambda_{max} \sim 600$ nm. A color change from red to blue also attested for the self-assembly.

Under addition of linker, the degree of colloidal association can be modulated from chainlike to dense **AuNPs-NOI**/**BPEB** clusters (Fig. 12). Unlike XB donor **AuNPs-NOI**, **AuNPs-NOF** have resulted inactive toward **BPEP** in a self-assembly process.[37]

In a second step, **AuNPs-NOX** were self-assembled on organic monolayers **M1** and **M2** where pyridyl functionalities

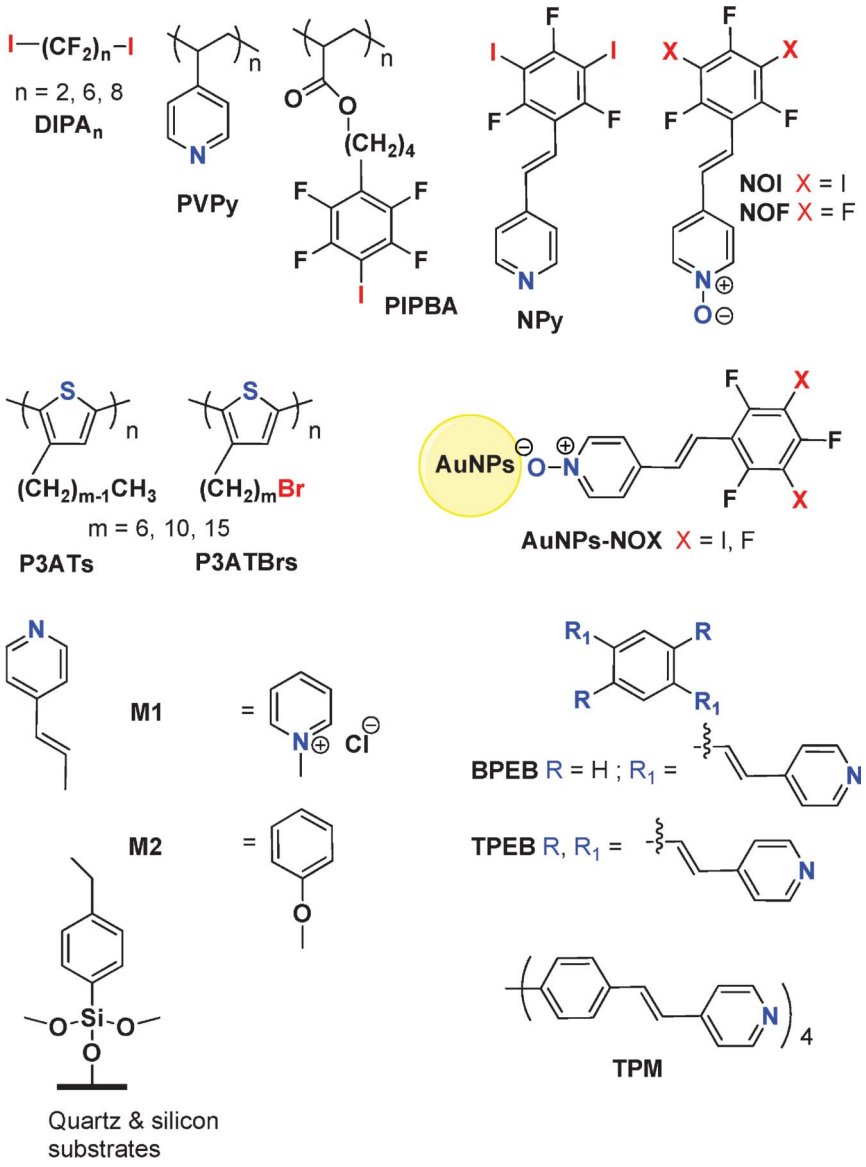

Fig. 10 Structures of polymers, cross-linkers, self-assembled mono-layers and coated nanoparticles.

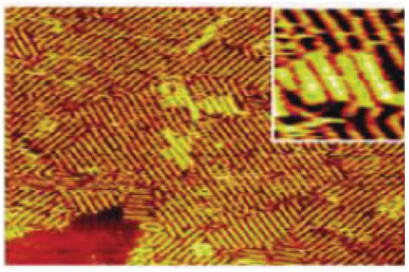

Fig. 11 Topographic STM image on HOPG of **P3TBr** at 9.77 × 10^{-6} M in phenyloctane (I_T = 240 pA, V_T = −1400 mV, 90 × 58 nm^2) with, inset, its corresponding zoom (I_T = 240 pA, V_T = −1400 mV, 10 × 10 nm^2). Reproduced with permission from the American Chemical Society.

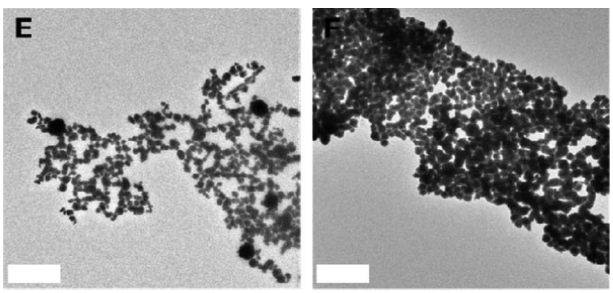

Fig. 12 TEM images of **AuNPs-NOI** with low (left) and high (right) concentrations of **BPEB**. The insets correspond to the enlarged areas with scale bars of 100 nm. Reproduced with permission from John Wiley and Sons.

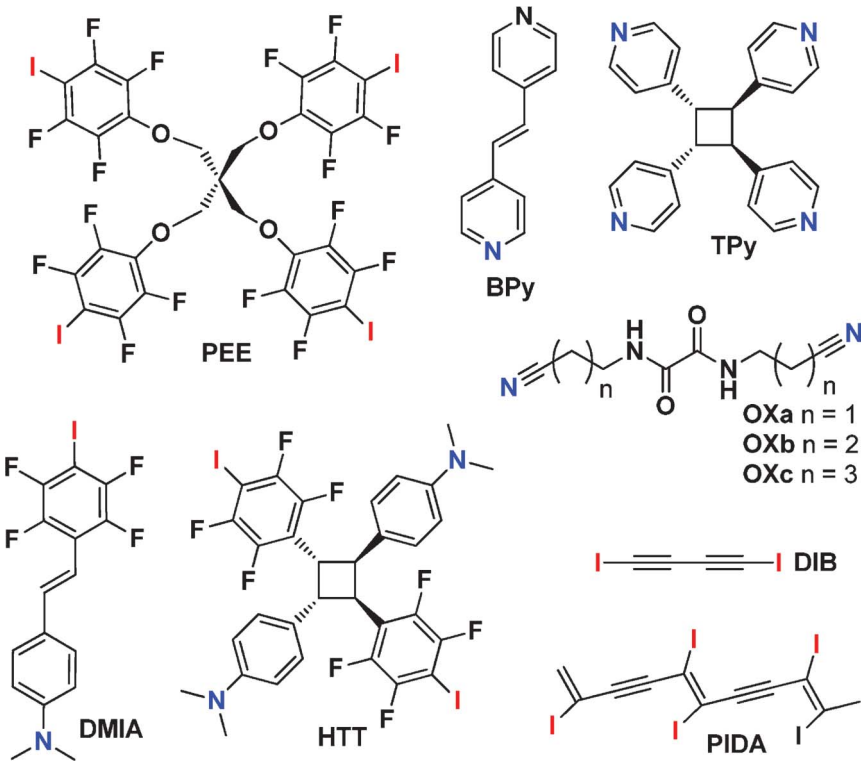

Fig. 13 Structures of templates, starting units and resulting materials involved in the solid state syntheses.

point at the outer surface. The AFM analysis exposed a uniform distribution of **AuNPs-NOX** on **M1** whereas **M2** is mostly covered with the iodinated AuNPs. While electrostatic interactions prevail over the XB factor in **M1**, the selectivity of XB dominates in **M2**. Then, a stepwise assembly of **AuNPs-NOI** on monolayers **M1** and **M2** was run in the presence of ditopic and tetratopic XB acceptor cross-linkers **BPEB**, **TPEB**, and **TPM**. After 3 and 6 **AuNPs-NOI** deposition steps, scanning electron microscopy (SEM) and AFM studies established an evolution of the film morphology governed by both the structure of the monolayer and the cross-linker geometry. The predominant role of XB was expressed by the absence of **AuNPs-NOF/BPEB** or **AuNPs-NOI** (without **BPEP**) extra layer on **M1** after further deposition steps, since **AuNPs-NOF/BPEB** or **AuNPs-NOI** have no (self-)complementarity.[38]

Solid state synthesis

The [2+2] photocyclization reaction in the solid state represents a distinctive mode of covalent bond formation in a regio and stereoselective manner. Thus, specific geometric criteria postulated by Schmidt outlined that a pair of olefinic bonds has to be aligned in a parallel fashion separated by a distance ranging 3.5 to 4.2 Å. To this end, Resnati and co-workers engineered a tetratopic XB donor **PEE** in order to pre-organize *trans*-1,2-bis(4-pyridyl)ethylene modules (**BPy**) in the desired supramolecular arrangement (Fig. 13).[39] The co-crystallization of compounds **PEE** and **BPy** in a 1 : 2 ratio provided suitable material for a single crystal X-ray diffraction analysis. Thus, interaction parameters are consistent with strong N···I halogen bonds operating between both partners, namely N···I distances of about 21% shorter than the sum of the van der Waals radii and almost linear N–I–C angle. The aromatic rings of the pentaerythritol ether (**PEE**) are also separated by a distance spanning from 3.524 to 3.897 Å, due to a π···π stacking. The infinite supramolecular structure was thereby comprised of pre-arranged olefins in a parallel fashion (double bond separation <4.5 Å), which fulfilled the topochemical postulate. The subsequent irradiation at 300 nm of the powdered crystalline material has yielded quantitatively the corresponding tetrakis(4-pyridyl)cyclobutane (**TPy**) as the sole *rctt* isomer. The pre-organization of olefins can also be realized by their functionalization with self-complementary groups (Fig. 13). In this regard, the facile crystallization of compound **DMIA** followed by a thorough X-ray analysis has disclosed the crystal packing. The telechelic heteroditopic modules are linked by N···I halogen bonds developing a wavy infinite chain. Moreover, they were paired in a head-to-tail mode thanks to π···π interactions between aromatic groups of opposite quadrupolar moments. The distance between the double bond centroids was 3.758 Å which meets the requirements for a [2+2] reaction in the solid state. After photoirradiation at 300 nm for 24 h, the chromophore **DMIA** was converted into the cycloadduct **HTT** in 80% yield, as determined by ^{1}H NMR spectroscopy. Likewise, the X-ray structure of heterotetratopic

module **HTT** confirmed a complete regio- and stereospecificity.[40]

Halogen bonding was also explored for achieving the topochemical 1,4-polymerization of diynes in the solid state. Unlike the [2+2] photoaddition, the structural parameters entail a repeat distance between units of 4.9 Å and an orientation angle of 45° relative to the translation axis. Moreover, a C1–C4 distance of 3.5 Å for successive diyne units favoured the 1,4-polymerization.[41] Taking advantage of the high directionality of XB, the polymerization under topochemical control of diiodobutadiyne (**DIB**) was examined in the presence of hosts **OXa** to **OXc** (Fig. 13). These templates acted concomitantly at two levels: (i) the hydrogen bonded oxalamide functionalities imparted a 1 dimensional self-organization to the overall structure and (ii) the nitrile end groups maintained the diynes in the desired face-to-face arrangement through weak halogen bondings. When challenged with diiodobutadiyne in a 1 : 1 ratio in methanol, only components **OXb** and **OXc** afforded co-crystals. As far as the crystal structure of complex **DIB-OXb** is concerned, the nitrile groups are effectively bound to the iodine atoms but a repeat distance of 5.25 Å has prevented the polymerization process (Fig. 14). In contrast, X-ray diffraction analysis of system formed from **DIB-OXc** showed only the poly(diiododiacetylene) (**PIDA**) linked to the host molecule, confirming the perfect topochemical arrangement in a roundabout way. Inferred from SEM measurements, the resulting **PIDA** was expected to be conductive with highly anisotropic electrical and optical properties.[42]

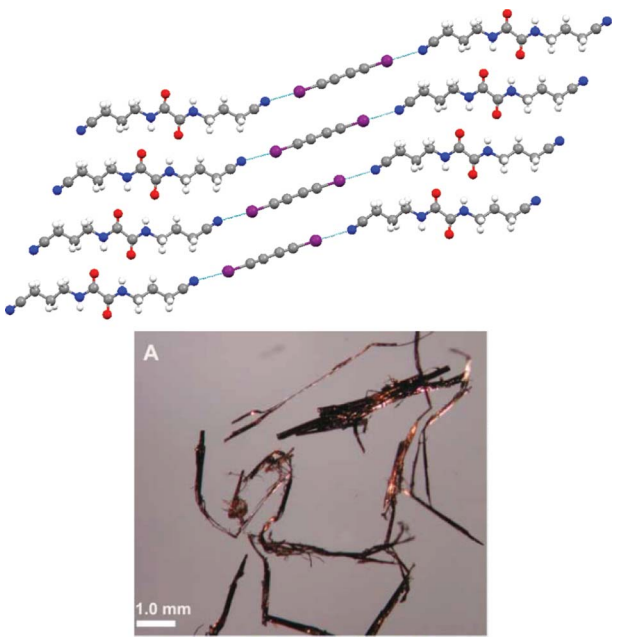

Fig. 14 X-ray structure of complex **DIB-OXb** (top). Microscopic image taken under polarized light of **PIDA** (bottom) Reproduced with permission from Science.

Catalytic systems

In the realm of organocatalysis, the structural design is mainly promoted by hydrogen bondings taking place in the activation of an electrophile towards a nucleophilic attack. Bolm and co-workers have therefore evaluated the halogen bonding as potential catalytic process due to a similar selectivity and directionality with the HB counterpart.[43] The target reaction consisted in the transfer hydrogenation of 2-phenylquinoline (**PhQa**) by Hantzsch ester (**He**) mediated by a C=N activation (Fig. 15). A set of bromo- and iodoperfluoroalkanes **HPFA**, **DPFA** was considered as catalysts under classical conditions, namely a 10 mol% content of haloperfluoroalkane in the presence of 2.2 equivalents of ester **He** in toluene or CH_2Cl_2. From these reactions, it was evidenced that the longer the chain length of **HPFA**, the higher the reactivity. In addition, better results were obtained with the iodo derivatives (yields rising to 98%), following the accepted trend I > Br for XB interaction strength. Only 1 mol% of perfluorohexyliodide even allowed the formation of tetrahydroquinoline **THQa** in 69% yield when the reaction proceeded in CH_2Cl_2 at 25 °C. Finally, perfluorooctyliodide was successfully used for the reduction of varied 2-substituted quinolines **PhQb** in tetrahydroquinoline **THQb**, yields being in the range 70 to 98%.

Another XB organocatalytic process was drawn on for a Ritter-like reaction. So, the substitution of a bromide atom for an amide group necessitates the activation of the C–Br bond. In this respect, iodoperfluoro compounds, used as XB catalyst, were first assessed in the formation of *N*-benzhydryl acetamide (**BHb**) from benzhydryl bromide (**BHa**) in deuterated acetonitrile (Fig. 15). However, the poor conversion has convinced the authors to elaborate new 2-iodoimidazolium derivatives **IMDa-c** as strong XB donors. According to the ^{1}H NMR monitoring, reactions performed with an equimolar amount of catalyst **IMDa-c** afforded a conversion of **BHa** into **BHb** in 80 to 97% yields. The coordinating effect of the counteranion was brought out by higher yields with BF_4 derivative **IMDc** in comparison to triflate **IMDa,b**, as a consequence of a stronger electron donation from TfO^- anion toward iodine. In addition, the use of the bromoimidazolium derivative **IMDd** as activating agent has resulted in a conversion of only 54% yields, following the aforementioned trend for XB interaction strength.[44]

Recently, the electrophilic activation of carbonyl groups by iodine trichloride ($\mathbf{ICl_3}$) was investigated in the frame of the selective and controlled ring opening polymerization (ROP) of L-lactide (**LA**) (Fig. 15). First, the prerequisite C=O···I halogen bonds between $\mathbf{ICl_3}$ and **LA** were evidenced in solution by infra-red and ^{13}C NMR spectroscopy measurements. Moreover, the inorganic catalyst was found to activate the nucleophilic initiator of ROP (11-bromo-1-undecanol, **11-BU**) through OH···Cl hydrogen bonds. Thus, the polymerization of **LA** was allowed to proceed at room temperature in chloroform using an initiator/catalyst ratio down to 1 : 1. However, an increase in the catalyst amount affected positively the polymerization parameters. When a **11-BU**/$\mathbf{ICl_3}$ ratio 1 : 15 was used, the

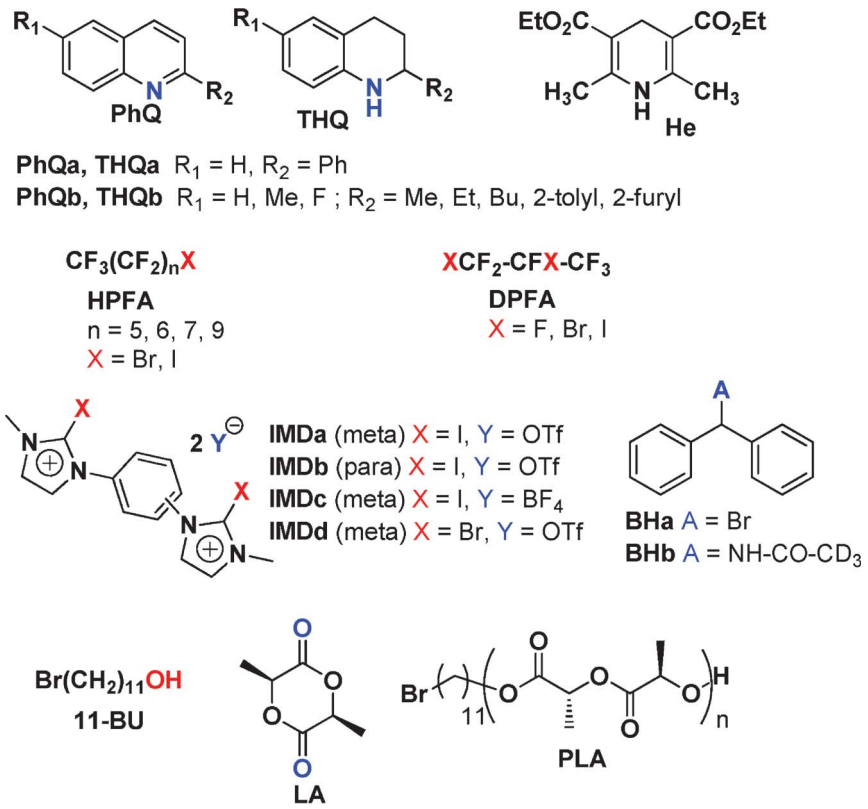

Fig. 15 Structures of catalysts, starting and final materials involved in XB based catalytic reactions.

poly(L-lactide) was isolated with a molecular weight of about 21 kg mol^{-1} and a polydispersity index of 1.4, as determined by gel permeation chromatography. In accordance with a controlled polymerization, an electrospray ionization mass spectrometry analysis corroborated the exclusive functionalization of polymer chains with **11-BU**.[45]

Recycling and resolution processes

From an economic, technical, safety and environmental standpoint, recycling and resolution processes have become key factors in synthetic chemistry. In this regard, the resolution of a racemic perfluorocarbon was mediated through XB diastereoisomeric adducts formation. Purposely, an equimolar amount of enantiopure (−)-sparteine hydrobromide

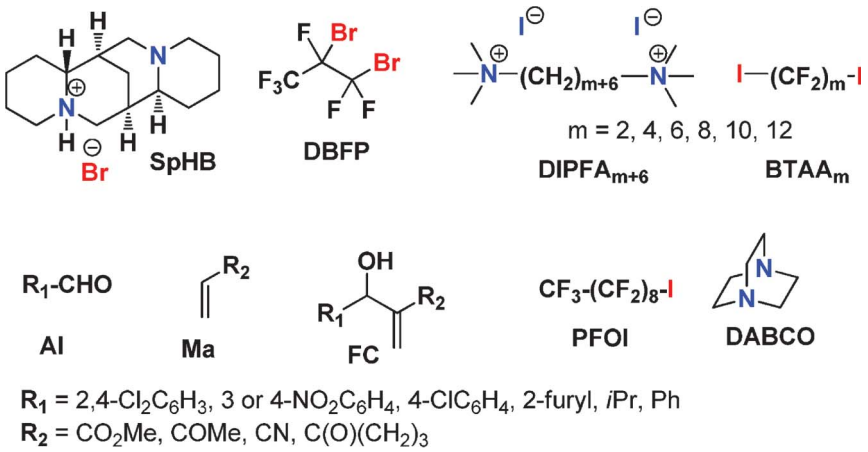

Fig. 16 Molecules involved in recycling and resolution processes.

(**SpHB**) and racemic 1,2-dibromohexafluoropropane (**DBFP**) was co-crystallized in chloroform, giving rise to yellow crystals with a higher melting point with respect to starting materials (Fig. 16). According to the single-crystal X-ray analysis, the self-assembly process has developed a helical architecture where bromide anions of **SpHB** are linked to bromide atoms of **DBFP** with separated distances of about 3.3 Å (~80% of the sum of the van der Waals radii). Interestingly, the mixture comprised exclusively the (*S*)-enantiomer of **DBFP**, affording, in that way, a chiral resolution process for racemic perfluorocarbons.[46]

In 2009, the resolution of α,ω-diiodoperfluoroalkanes (**DIPFA$_m$**) mixtures using bis(trimethylammonium) alkane diiodides (**BTAA$_{m+6}$**) was reported in a selective and reversible mode (Fig. 16). All **DIPFA$_m$** were able to crystallize with **BTAA$_{m+6}$**, however, the crystal packing of resulting complexes has differed dramatically. Indeed, a good size matching was observed for compounds **BTAA$_{m+6}$** and **DIPFA$_m$**, namely N^+–N^+ (intramolecular distances)/ I^-–I^- (in $I^-\cdots I(CF_2)_nI\cdots I^-$ super-anions) distances varying from 0.69 to 0.85 Å. Afterwards, a solution of one equivalent of each **DIPFA$_m$** was mixed with one equivalent of one single **BTAA$_{m+6}$** salt. The competitive crystallization studies have resulted in the sole crystallization of the size-matched **DIPFA$_m$**, *i.e.* the **BTAA$_{m+6}$·DIPFA$_m$** partners (Fig. 17). In addition, a controlled release of **DIPFA$_m$** was conducted under heating which has yielded the starting **BTAA$_{m+6}$** salts in their initial crystal lattice. Further experiments were performed in the vapour phase. When exposed to vapour of matched **DIPFA$_m$**, nonporous ionic solids **BTAA$_{m+6}$** were allowed to encapsulate the host **DIPFA$_m$** with the same above mentioned crystal lattice. Under the same conditions, matched **DIPFA$_m$** was capable of substituting the mismatched **DIPFA$_m$** in a mismatched complex. Thus, these impressive gas-solid reactions combined a controlled and selective absorption and release of molecules to a recycling process of **BTAA** guests.[47]

A recycling procedure of **DABCO** organocatalyst was also considered in the frame of the Morita–Baylis–Hillman reaction (Fig. 16). A first step has consisted in the formation of a supramolecular complex comprised of **DABCO** bound to two perfluorooctyl iodide units (**PFOI**) by N···I halogen bonds, which could be recovered by simple filtration. After analytical evidence of the XB nature of the interactions, the new **DABCO·PFOI** catalyst was able to promote Morita–Baylis–Hillman reactions under classical conditions: a 10 mol% content of **DABCO·PFOI** with Michael acceptors **Ma** and aldehydes **Al** in addition to 2 equivalents of methanol. With the exception of *i*-butyraldehyde as the starting reagent, the reactions involving **Ma** and **Al** led to compounds **FC** in yields up to 92%. Then, a multi gram scale synthesis has pointed out the recycling feasibility by recovering the **DABCO·PFOI** catalyst under precipitation and filtration procedures. The persistent activity of recovered **DABCO·PFOI** was also verified in up to five repeated sequences.[48]

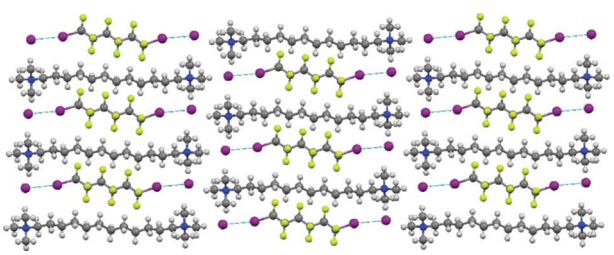

Fig. 17 X-Ray structure of complex **BTAA$_{12}$·DIPFA$_6$**.

Conclusions

Over the last decade, halogen bonding (XB) has gained tremendous interest for the construction of supramolecular complexes by crystal engineering. While applications of hydrogen bonding in various research areas such as materials science and synthetic chemistry are abundant, only a handful of instances were purposely built upon halogen bonding. However, the combination of an exquisite neutral and ionic sensitivity and a high directionality makes the development of halogen bonded systems only in its infancy. Here, we presented the first applications in the field of highly functional materials through a remarkable series of electronic and photoresponsive components. On a parallel scene, XB in the solution phase recognition has arisen in anion sensing, catalysis and resolution processes, highlighting a reliable selectivity. In addition, the weak intermolecular phenomenon was able to govern the organization of species at the macromolecular level as observed in coatings, and the self-assembly of polymer and hybrid systems. Beyond the formation of exclusive halogen bonded complexes, the potential cooperation between weak non-covalent bonds thereby opens new perspectives in materials science and synthetic chemistry and accounts for new challenges for chemist imagination.

References

1 *Supramolecular Chemistry: from molecules to nanomaterials*; ed. P. A. Gale and J. W. Steed; John Wiley & Sons, Ltd, 2012.
2 (*a*) Halogen Bonding, Fundamentals and Applications; ed. P. Metrangolo and G. Resnati; *Structure and Bonding,* Vol. 126; Springer Verlag: Berlin Heidelberg, 2008; (*b*) P. Metrangolo and G. Resnati, *Science*, 2008, **321**, 918; (*c*) P. Metrangolo, F. Meyer, T. Pilati, G. Resnati and G. Terraneo, *Angew. Chem., Int. Ed.*, 2008, **47**, 6114.
3 O. Hassel, *Science*, 1970, **170**, 497.
4 (*a*) Y. Lu, T. Shi, Y. Wang, H. Yang, X. Yan, X. Luo, H. Jiang and W. Zhu, *J. Med. Chem.*, 2009, **52**, 2854; (*b*) E. Parisini, P. Metrangolo, T. Pilati, G. Resnati and G. Terraneo, *Chem. Soc. Rev.*, 2011, **40**, 2267; (*c*) M. Carter and P. S. Ho, *Cryst. Growth Des.*, 2011, **11**, 5087; (*d*) L. A. Hardegger, B. Kuhn, B. Spinnler, L. Anselm, R. Ecabert, M. Stihle, B. Gsell, R. Thoma, J. Diez, J. Benz, J.-M. Plancher, G. Hartmann, D. W. Banner, W. Haap and F. Diederich, *Angew. Chem., Int. Ed.*, 2011, **50**, 314; (*e*) Y. Lu, Y. Liu, Z. Xu, H. Li, H. Liu and W. Zhu, *Expert Opin. Drug Discovery*, 2012, **7**, 375.

5 (*a*) K. Rissanen, *CrystEngComm*, 2008, **10**, 1107; (*b*) L. Brammer, G. M. Espallargas and S. Libri, *CrystEngComm*, 2008, **10**, 1712; (*c*) P. Politzer, J. S. Murray and T. Clark, *Phys. Chem. Chem. Phys.*, 2010, **12**, 7748.
6 H. Loc Nguyen, P. N. Horton, M. B. Hursthouse, A. C. Legon and D.W. Bruce, *J. Am. Chem. Soc.*, 2004, **126**, 16.
7 J. Xu, X. Liu, T. Lin, J. Huang and C. He, *Macromolecules*, 2005, **38**, 3554.
8 J. Xu, X. Liu, J. Kok-Peng, T. Lin, J. Huang and C. He, *J. Mater. Chem.*, 2006, **16**, 3540.
9 P. Metrangolo, C. Präsang, G. Resnati, R. Liantonio, A. C. Whitwood and D. W. Bruce, *Chem. Commun.*, 2006, 3290.
10 D. W. Bruce, P. Metrangolo, F. Meyer, C. Präsang, G. Resnati, G. Terraneo and A. C. Whitwood, *New J. Chem.*, 2008, **32**, 477.
11 C. Präsang, A. C. Whitwood and D. W. Bruce, *Chem. Commun.*, 2008, 2137.
12 E. Corradi, S. V. Meille, M. T. Messina, P. Metrangolo and G. Resnati, *Angew. Chem., Int. Ed.*, 2000, **39**, 1782.
13 C. Präsang, H. L. Nguyen, P. N. Horton, A. C. Whitwood and D. W. Bruce, *Chem. Commun.*, 2008, 6164.
14 D. W. Bruce, P. Metrangolo, F. Meyer, T. Pilati, C. Präsang, G. Resnati, G. Terraneo, S. G. Wainwright and A. C. Whitwood, *Chem.–Eur. J.*, 2010, **16**, 9511.
15 E. Cariati, A. Forni, S. Biella, P. Metrangolo, F. Meyer, G. Resnati, S. Righetto, E. Tordin and R. Ugo, *Chem. Commun.*, 2007, 2590.
16 E. Cariati, G. Cavallo, A. Forni, G. Leem, P. Metrangolo, F. Meyer, G. Resnati, S. Righetto, G. Terraneo and E. Tordin, *Cryst. Growth Des.*, 2011, **11**, 5642.
17 A. Priimagi, G. Cavallo, A. Forni, M. Gorynsztejn–Leben, M. Kaivola, P. Metrangolo, R. Milani, A. Shishido, T. Pilati, G. Resnati and G. Terraneo, *Adv. Funct. Mater.*, 2012, **22**, 2572.
18 O. Bolton, K. Lee, H. J. Kim, K. Y. Lin and J. Kim, *Nat. Chem.*, 2011, **3**, 205.
19 (*a*) Y. Hosokoshi, M. Tamura, K. Nozawa, S. Suzuki, M. Kinishita, H. Sawa and R. Kato, *Synth. Met.*, 1995, **71**, 1795; (*b*) T. Imakubo, H. Sawa and R. Kato, *Synth. Met.*, 1995, **73**, 117.
20 (*a*) ''Halogen bonding in conducting or magnetic molecular materials'' M. Fourmigué, *from Structure and Bonding* Vol. 126; Springer Verlag: Berlin Heidelberg, 2008, pp181–207; (*b*) M. Fourmigué and P. Batail, *Chem. Rev.*, 2004, **104**, 5379.
21 K.-S. Shin, M. Brezgunova, O. Jeannin, T. Roisnel, F. Camerel, P. Auban-Senzier and M. Fourmigué, *Cryst. Growth Des.*, 2011, **11**, 5337.
22 (*a*) P. Metrangolo, T. Pilati, G Terraneo, S. Biella and G. Resnati, *CrystEngComm*, 2009, **11**, 1187; (*b*) G. Cavallo, P. Metrangolo, T. Pilati, G. Resnati, M. Sansotera and G. Terraneo, *Chem. Soc. Rev.*, 2010, **39**, 3772.
23 A. Mele, P. Metrangolo, H. Neukirch, T. Pilati and G. Resnati, *J. Am. Chem. Soc.*, 2005, **127**, 14972.
24 (*a*) M. G. Sarwar, B. Dragisic, S. Sagoo and M. S. Taylor, *Angew. Chem., Int. Ed.*, 2010, **49**, 1674; (*b*) E. Dimitrijević, O. Kvak and M. S. Taylor, *Chem. Commun.*, 2010, **46**, 9025.
25 M. G. Chudzinski, C. A. McClary and M. S. Taylor, *J. Am. Chem. Soc.*, 2011, **133**, 10559.
26 A. Caballero, N. G. White and P. D. Beer, *Angew. Chem., Int. Ed.*, 2011, **50**, 1845.
27 (*a*) N. L. Kilah, M. D. Wise and P. D. Beer, *Cryst. Growth Des.*, 2011, **11**, 4565; (*b*) A. Vargas Jentzsch, D. Emery, J. Mareda, P. Metrangolo, G. Resnati and S. Matile, *Angew. Chem., Int. Ed.*, 2011, **50**, 11675; (*c*) S. M. Walter, F. Kniep, L. Rout, F. P. Schmidtchen, E. Herdtweck and S. M. Huber, *J. Am. Chem. Soc.*, 2012, **134**, 8507; (*d*) F. Zapata, A. Caballero, N. G. White, T. D. W. Claridge, P. J. Costa, V. Félix and P. D. Beer, *J. Am. Chem. Soc.*, 2012, **134**, 11533; (*e*) A. Vargas Jentzsch, D. Emery, J. Mareda, S. K. Nayak, P. Metrangolo, G. Resnati, N. Sakai and S. Matile, *Nat. Commun.*, 2012, **3**, 905.
28 T. Takeuchi, Y. Minato, M. Takase and H. Shinmori, *Tetrahedron Lett.*, 2005, **46**, 9025.
29 A mutual induced fitting process provided exclusively 6.3 honeycomb networks whether the cation shape of onium salts matched with the hexagonal cavity: P. Metrangolo, F. Meyer, T. Pilati, G. Resnati and G. Terraneo, *Chem. Commun.*, 2008, 1635.
30 F. C. Pigge, V. R. Vangala, P. P. Kapadia, D. C. Swenson and N. P. Rath, *Chem. Commun.*, 2008, 4726.
31 K. Raatikainen and K. Rissanen, *CrystEngComm*, 2011, **13**, 6972.
32 K. Raatikainen and K. Rissanen, *Chem. Sci.*, 2012, **3**, 1235.
33 R. Bertani, P. Metrangolo, A. Moiana, E. Perez, T. Pilati, G. Resnati, L. Rico-Lattes and A. Sassi, *Adv. Mater.*, 2002, **14**, 1197.
34 F. Wang, N. Ma, Q. Chen, W. Wang and L. Wang, *Langmuir*, 2007, **23**, 9540.
35 T. Shirman, D. Freeman, Y. Diskin Posner, I. Feldman, A. Facchetti and M. E. van der Boom, *J. Am. Chem. Soc.*, 2008, **130**, 8162.
36 A. Bocheux, I. Tahar-Djebbar, C. Fiorini-Debuisschert, L. Douillard, F. Mathevet, A.-J. Attias and F. Charra, *Langmuir*, 2011, **27**, 10251.
37 T. Shirman, T. Arad and M. E. van der Boom, *Angew. Chem., Int. Ed.*, 2010, **49**, 926.
38 T. Shirman, R. Kaminker, D. Freeman and M. E. van der Boom, *ACS Nano*, 2011, **5**, 6553.
39 T. Caronna, R. Liantonio, T. A. Logothetis, P. Metrangolo, T. Pilati and G. Resnati, *J. Am. Chem. Soc.*, 2004, **126**, 4500.
40 G. Marras, P. Metrangolo, F. Meyer, T. Pilati, G. Resnati and A. Vij, *New J. Chem.*, 2006, **30**, 1397.
41 N. S. Goroff, S. M. Curtis, J. A. Webb, F. W. Fowler and J. W. Lauher, *Org. Lett.*, 2005, **7**, 1891.
42 A. Sun, J. W. Lauher and N. S. Goroff, *Science*, 2006, **312**, 1030.
43 A. Bruckmann, M. A. Pena and C. Bolm, *Synlett*, 2008, **6**, 900.
44 S. M. Walter, F. Kniep, E. Herdtweck and S. M. Huber, *Angew. Chem., Int. Ed.*, 2011, **50**, 7187.
45 O. Coulembier, F. Meyer and P. Dubois, *Polym. Chem.*, 2010, **1**, 434.
46 A. Farina, S. V. Meille, M. Teresa Messina, P. Metrangolo, G. Resnati and G. Vecchio, *Angew. Chem., Int. Ed.*, 1999, **38**, 2433.
47 P. Metrangolo, Y. Carcenac, M. Lahtinen, T. Pilati, K. Rissanen, A. Vij and G. Resnati, *Science*, 2009, **323**, 1461.
48 S. Dordonne, B. Crousse, D. Bonnet-Delpon and J. Legros, *Chem. Commun.*, 2011, **47**, 5855.